Check for updates

JGR Space Physics

RESEARCH ARTICLE
10.1029/2024JA032724

# Impact of the Polar Vortex on Sub-Seasonal $O/N_2$ Variability in the Lower Thermosphere Using GOLD and WACCM-X

**Benjamin C. Martinez[1], Xian Lu[1], Nicholas M. Pedatella[2], Haonan Wu[1,2], and Jens Oberheide[1]**

[1]Department of Physics and Astronomy, Clemson University, Clemson, SC, USA, [2]High Altitude Observatory, NSF National Center for Atmospheric Research, Boulder, CO, USA

**Key Points:**

- Polar vortex (PV) activity is correlated with sub-seasonal $O/N_2$ variability during low Kp winter times at all latitudes
- We observe enhanced $O/N_2$ at high southern latitudes and reduced $O/N_2$ at low latitudes in response to northern hemisphere PV activity
- PV-$O/N_2$ correlations are shown to reflect PV induced modulations of the residual mean meridional circulation (MMC)

**Correspondence to:**

B. C. Martinez,
ben8@g.clemson.edu

**Citation:**

Martinez, B. C., Lu, X., Pedatella, N. M., Wu, H., & Oberheide, J. (2024). Impact of the polar vortex on sub-seasonal $O/N_2$ variability in the lower thermosphere using GOLD and WACCM-X. *Journal of Geophysical Research: Space Physics*, *129*, e2024JA032724. https://doi.org/10.1029/2024JA032724

Received 5 APR 2024
Accepted 11 JUN 2024

**Author Contributions:**

**Conceptualization:** Benjamin C. Martinez, Xian Lu, Jens Oberheide
**Data curation:** Benjamin C. Martinez, Haonan Wu
**Formal analysis:** Benjamin C. Martinez, Xian Lu
**Funding acquisition:** Xian Lu, Jens Oberheide
**Investigation:** Benjamin C. Martinez, Xian Lu, Nicholas M. Pedatella, Haonan Wu, Jens Oberheide
**Methodology:** Benjamin C. Martinez, Xian Lu, Nicholas M. Pedatella, Jens Oberheide
**Project administration:** Xian Lu
**Resources:** Xian Lu, Nicholas M. Pedatella, Haonan Wu
**Software:** Haonan Wu
**Supervision:** Xian Lu
**Validation:** Benjamin C. Martinez, Xian Lu, Nicholas M. Pedatella

©2024. The Author(s).
This is an open access article under the terms of the Creative Commons Attribution License, which permits use, distribution and reproduction in any medium, provided the original work is properly cited.

**Abstract** We provide observational evidence that the stability of the stratospheric Polar vortex (PV) is a significant driver of sub-seasonal variability in the thermosphere during geomagnetically quiet times when the PV is anomalously strong or weak. We find strong positive correlations between the Northern Annular Mode (NAM) index and subseasonal (10–90 days) Global Observations of the Limb and Disk (GOLD) $O/N_2$ perturbations at low to mid-northern latitudes, with a largest value of +0.55 at ∼30.0°N when anomalously strong or weak (NAM >2.5 or < −2.1) vortex times are considered. Strong agreement for $O/N_2$ variability and $O/N_2$-NAM correlations is found between GOLD observations and the Whole Atmosphere Community Climate Model with thermosphere-ionosphere eXtension (WACCM-X) simulations, which is then used to delineate the global distribution of $O/N_2$-NAM correlations. We find negative correlations between subseasonal variability in WACCM-X $O/N_2$ and NAM at high northern and southern latitudes (as large as −0.54 at ∼60.0°S during anomalous vortex times). These correlations suggest that PV driven upwelling at low latitudes is accompanied by corresponding downwelling at high latitudes in the lower thermosphere (∼80–120 km), which is confirmed using calculations of residual mean meridional circulation from WACCM-X.

**Plain Language Summary** The stratospheric Polar vortex (PV) is a large-scale circulation pattern that forms over the poles during the winter months, characterized by strong winds circulating in a counterclockwise direction in the Northern Hemisphere. It has previously been demonstrated that the breakup of the PV during sudden stratospheric warming (SSW) events has a large effect on the composition of the thermosphere. We demonstrate that the PV also influences thermospheric composition during non-SSW times, including time periods in which the vortex is strong and times in which the vortex is inactive, by correlating observations of thermospheric $O/N_2$ from the Global Observations of the Limb and Disk (GOLD) instrument with the Northern Annular Mode (NAM) index, which tracks the strength of the PV. We also find strong anti-correlations between $O/N_2$ and tidal amplitudes from model simulations, which suggests that the PV influences thermospheric composition via changes in mean circulation induced by the dissipation of enhanced waves. We use model simulations to confirm that the NAM-$O/N_2$ correlations reflect PV induced changes in global circulation patterns. We find that the PV causes enhanced upwelling at low latitudes and corresponding downwelling at high latitudes in both the northern and southern hemispheres.

## 1. Introduction

The column number density ratio of atomic oxygen to molecular nitrogen is a commonly used parameter to represent the composition of the thermosphere (Strickland et al., 1995). This parameter varies on a wide range of time scales, from diurnal and day-to-day variations to seasonal, solar cycle, and longer time scale variations resulting from, for example, solar extreme ultraviolet (EUV), plasma-neutral collisions, and Joule heating (Luan et al., 2017; Yu et al., 2020). Subseasonal variations in $O/N_2$ can, therefore, be used to track the subseasonal variability of the ionosphere-thermosphere (IT) region. $O/N_2$ is highly sensitive to geomagnetic activity, particularly at high latitudes and during geomagnetically active times (Martinez & Lu, 2023), but $O/N_2$ variability at low and mid-latitudes during geomagnetically quiet times has also been shown to be modulated primarily by *in-situ* generated tides and/or upward-propagating waves originating from the lower atmosphere (England et al., 2010; England & Greer et al., 2021; England & Meier et al., 2021; Zhang et al., 2010).

Tides and planetary waves in the Northern Hemisphere winter are strongly influenced by the cyclonic stratospheric Polar vortex (PV), which is itself highly variable in terms of both wind speeds and the extent of the cyclone (Labitzke & Naujokat, 2000; Pedatella & Harvey, 2022). The strength of the PV can be quantified by the

21699402, 2024, 6, Downloaded from https://agupubs.onlinelibrary.wiley.com/doi/10.1029/2024JA032724, Wiley Online Library on [29/07/2024]. See the Terms and Conditions (https://onlinelibrary.wiley.com/terms-and-conditions) on Wiley Online Library for rules of use; OA articles are governed by the applicable Creative Commons License

**Visualization:** Benjamin C. Martinez
**Writing – original draft:** Benjamin C. Martinez, Xian Lu
**Writing – review & editing:** Benjamin C. Martinez, Xian Lu, Nicholas M. Pedatella, Haonan Wu, Jens Oberheide

Northern Annular Mode (NAM) index, where a low NAM corresponds to a weaker vortex and a high NAM corresponds to a stronger vortex (Baldwin, 2001; Thompson & Wallace, 2000). When the PV is strong, it has a well-defined, nearly circular shape that is constrained to high northern latitudes, but when the vortex is weak, it develops an irregular shape that penetrates to mid-latitudes. During winter months, enhancements in tropospheric planetary wave activity, and their interactions with the mean winds, can cause the vortex to weaken leading to sudden stratospheric warming (SSW) events (Matsuno, 1971). SSWs can dramatically impact the whole atmosphere, including significant effects on the ionosphere and thermosphere (Baldwin et al., 2021; Goncharenko et al., 2021). The effects of SSWs on the global distribution of thermospheric $O/N_2$ were shown in TIE-GCM simulations by Pedatella et al. (2016) and confirmed observationally by Oberheide et al. (2020), in which a ∼10% depletion in the $O/N_2$ column density ratio was observed in both hemispheres in response to the 2019 SSW. In these studies, the low latitude depletion in $O/N_2$ was attributed to the enhanced wave driving of residual mean circulation, resulting in changes in the concentration of O in the lower thermosphere. These changes then propagate into the upper thermosphere via molecular diffusion.

Recently, Pedatella (2023) demonstrated the influence of the PV (outside SSW) on $O/N_2$ from a modeling standpoint by finding positive correlations between the NAM index and $O/N_2$ residuals extracted from an ensemble of 40 northern hemisphere winters simulated by the Whole Atmosphere Community Climate Model with thermosphere-ionosphere eXtension (WACCM-X) in its free-running mode. Additionally, Greer et al. (2023) performed a case study of the response of $O/N_2$, among other ionospheric and thermospheric parameters, to PV variability during one period of weak vortex activity (February 2008) and one period of strong vortex activity (February 2021) using data from the Thermosphere, Ionosphere, Mesosphere, Energetics, and Dynamics (TIMED) Global UltraViolet Imager (GUVI) instrument. They found enhanced tidal activity during weak vortex times, with corresponding depletions in $O/N_2$ at low latitudes (and the opposite for the strong vortex case). They then used SD-WACCM-X simulations to attribute these enhancements/depletions in $O/N_2$ to circulation changes driven by the dissipation of enhanced/reduced tides. The results of both of these studies are consistent with the results of the statistical study presented here.

Here, we quantify the contribution of the PV to the variability of $O/N_2$ in the IT using observations from the Global Observations of the Limb and Disk (GOLD) instrument for all winters from December 2018 to February 2023, with a goal of providing observational support for the simulation results of Pedatella (2023) and statistical support for the observational results of Greer et al. (2023). From a modeling standpoint, we further investigate the dependence of residual MMC on PV activity. We confirm that the correlations reported here accurately reflect modulations in global circulation arising from vortex driven wave activity.

This manuscript is organized as follows: Section 2 provides background on the GOLD $O/N_2$ data set and the SD-WACCM-X model used in this study, Section 3 provides a quantification of the influence of the PV on subseasonal (10–90 days) thermospheric variability from both an observational and modeling standpoint, and Section 4 demonstrates the influence of the PV on mean circulation that is responsible for the $O/N_2$-NAM correlations shown in Section 3.

## 2. Data and Methodology

### 2.1. GOLD Measurements

GOLD is in a geostationary orbit located at 47.5° W and observes the ratio of the vertical column density of O relative to $N_2$ defined at a standard reference $N_2$ depth of $10^{17}$ $cm^{-2}$ (Eastes et al., 2017). This reference depth is chosen to minimize uncertainty in $O/N_2$ as a function of 135.6 nm/LBH and is equivalent to ∼4 nbar, or ∼135 km (Correira et al., 2021). The $O/N_2$ ratio is retrieved directly from dayside disk measurements of the OI-135.6 nm and $N_2$-LBH band emission lines in the ∼134–164 nm wavelength range. We use version four of the $O/N_2$ data product. The GOLD $O/N_2$ data product is not optimized for auroral latitudes, so we limit our analysis to ±60° latitude. The observations have longitudinal coverage ranging from 113.5°W to 19.5°E and are only available during daytime.

We use version v04 of the GOLD $O/N_2$ data during all winters (defined as December, January, and February) from January 2019 to February 2023 and universal time (UTC) = ∼14:00–15:00 are used for the current study. This UTC range is chosen because the full field of view (FOV) of GOLD is illuminated at this time. GOLD scanned at a cadence of one full disk every half hour from 2019 to 2021, and every hour from 2022 onwards. For a

21699402, 2024, 6, Downloaded from https://agupubs.onlinelibrary.wiley.com/doi/10.1029/2024JA032724, Wiley Online Library on [29/07/2024]. See the Terms and Conditions (https://onlinelibrary.wiley.com/terms-and-conditions) on Wiley Online Library for rules of use; OA articles are governed by the applicable Creative Commons License

particular UTC, there is a 2-D snapshot image of the $O/N_2$ provided by GOLD for each individual day. In order to spatially suppress the noise, we take the average $O/N_2$ ratio in a 10° × 10° (longitude × latitude) grid box and attribute this value to the center of the grid. To study the subseasonal (10–90 days) variations in $O/N_2$, we calculate perturbations using a 10- to 90-day, fourth order, Butterworth bandpass filter.

It should be noted that GOLD $O/N_2$ measurements change abruptly during a Gyrating Yaw Mechanism (GYM) actuation, in which the GYM is moved to mitigate the effects of detector burn-in (see the GOLD instrument documentation, available at https://gold.cs.ucf.edu/). GYM actuations are performed several times per year. However, the GYM maneuvers do not significantly impact our results because we keep only data during active vortex, geomagnetically quiet winter times, and no GYM maneuvers occurred on or near the days that matched our strict geomagnetic and PV activity thresholds (see the end of Section 2.3 for more information on PV activity thresholds). Specifically, we do not use GOLD $O/N_2$ measurements from 5 days preceding or 15 days following a GYM maneuver. Good agreement between the $O/N_2$-NAM correlations from GOLD and those from SD-WACCM-X (where, of course, no impacts from instrumentation adjustments are included) further indicate that GYM actuations do not significantly impact our results (see Section 3.3).

### 2.2. SD-WACCM-X

The specified dynamics (SD) WACCM-X (SD-WACCM-X, hereafter referred to as WACCM-X), version 2.1, is a whole atmosphere model extending from the surface to an altitude of approximately 500 km based on the WACCM version 4 (Liu et al., 2018). The model has a horizontal resolution of 1.9° in latitude and 2.5° in longitude, and a vertical resolution of ∼1–3 km in the troposphere-stratosphere, and 0.25 scale heights above 0.96 hPa (∼50 km). The meteorology of the specified dynamics (SD) version of the model used in this study is constrained up to 50 km by the National Aeronautics and Space Administration (NASA) Modern-Era Retrospective analysis for Research and Applications version 2 (MERRA-2).

The column ratio of $O/N_2$ is calculated up to a reference $N_2$ depth of $10^{17}$ $cm^{-2}$ for consistency with GOLD measurements of $O/N_2$. Seasonal time-scale variations in $O/N_2$ are well captured by the model, as was demonstrated by Liu et al., 2023, who showed good overall agreement and high positive correlations at all latitudes between WACCM-X $O/N_2$ and GOLD $O/N_2$ observations during geomagnetically quiet times. The model run used in this study is from January 2010 to December 2022 and we use data for all winters. For consistency with GOLD observations, daily snapshots at UT = 14:00 are selected from the model. Perturbations in WACCM-X $O/N_2$ are again calculated using a 10- to 90-day Butterworth bandpass filter. Unlike the GOLD data set, the WACCM-X data set used here spans an entire solar cycle. The longer timeframe for the model data set was chosen in order to improve the statistics of our results. Although the two data sets are subject to different levels of solar activity, the bias that this would otherwise have introduced should be largely removed by the Butterworth filters. The strong agreement between correlations calculated using model data and observational data suggests that any remaining solar cycle impacts do not significantly impact/bias our analysis after filtering.

### 2.3. NAM Index

The dominant internal variability of the extratropical atmosphere in the northern hemisphere is characterized by the NAM index. For this study, NAM indices were calculated following the method of Gerber and Martineau (2018), using polar cap geopotential height anomalies from the NASA MERRA-2 reanalysis (Gelaro et al., 2017) at a pressure level of 10 hPa (∼30 km), at which internal variability is dominated by the variability of the PV. The NAM index is essentially a difference between geopotential anomalies at polar latitudes and mid-latitudes, such that a positive NAM is indicative of low pressure at polar latitudes and higher pressure at middle and low latitudes. Conversely, a negative NAM is indicative of high pressure at polar latitudes and lower pressure at middle and low latitudes. The cyclonic winds of the PV strengthen with decreasing pressure at the center, therefore a more positive NAM (low pressure at polar latitudes) corresponds to a stronger vortex and a more negative NAM (high pressure at polar latitudes) corresponds to a weaker vortex.

The NAM index quantifies vacillations in the position of the tropospheric jet streams and the strength of the stratospheric polar vortices, so it can be used to track the influence of the PV on $O/N_2$ by correlating the index with $O/N_2$ during the northern hemisphere winters when the PV is variable. We, therefore, limit our correlation analysis only to winter times, where we define the winter as times in which the PV is active/variable. We consider the vortex to be active when the standard deviation of the NAM index exceeds 0.35 within a 10-day rolling

21699402, 2024, 6, Downloaded from https://agupubs.onlinelibrary.wiley.com/doi/10.1029/2024JA032724, Wiley Online Library on [29/07/2024]. See the Terms and Conditions (https://onlinelibrary.wiley.com/terms-and-conditions) on Wiley Online Library for rules of use; OA articles are governed by the applicable Creative Commons License

**Table 1**
*Number of Winter Days, Days of Quiet Geomagnetic Activity (Daily Mean Kp < 2.0), Days With Polar Vortex (PV) Anomalously Strong (NAM ≥ 2.5) and/or Anomalously Weak (NAM ≤−2.1), and Days With Both Geomagnetically Quiet and Anomalous PV, for Different Years of GOLD Measurements, Total GOLD, and Total WACCM-X Data*

| | GOLD (2018–2023) | | | | | | |
|---|---|---|---|---|---|---|---|
| | 2018–2019 | 2019–2020 | 2020–2021 | 2021–2022 | 2022–2023 | Total (GOLD, 2018–2023) | Total (WACCM-X, 2010–2022) |
| Dates | Dec 15–Mar 25 | Nov 17–Mar 27 | Dec 10–Mar 20 | Dec 10–Mar 22 | Nov 27–Mar 14 | n/a | n/a |
| Winter days | 99 | 130 | 99 | 101 | 106 | 535 | 1,284 |
| Quiet days (Kp < 2.0) | 39 | 68 | 43 | 21 | 10 | 181 | 469 |
| Anomalous NAM days | 36 | 32 | 22 | 25 | 18 | 111 | 223 |
| NAM >2.5 days | 10 | 32 | 0 | 25 | 0 | 67 | 111 |
| NAM < −2.0 days | 26 | 0 | 22 | 0 | 18 | 66 | 134 |
| Quiet and anomalous NAM | 13 | 16 | 14 | 3 | 0 | 46 | 91 |

window. The start and end day for each winter based on this criterion, along with the number of geomagnetically quiet and/or anomalous vortex days included for each winter in which we have GOLD data is summarized in Table 1. Table 2 is similar to Table 1, except it contains information about the years for which we have data from WACCM-X, but no GOLD data. We define winter times based on a rolling standard deviation in order to increase the number of days (as compared to using only DJF) in our analysis maintaining a criterion of substantial PV variability. −2.1 and + 2.5 are approximately one standard deviation below and above the mean NAM value for geomagnetically quiet wintertimes, and so these values are selected as thresholds for anomalous NAM activity. Note that NAM values during these time periods are not symmetrically distributed around 0, hence our thresholds for anomalous NAM activity are not symmetric about 0, either. The selected thresholds were also found to maximize correlations between $O/N_2$ perturbations and the NAM index while still maintaining enough data for statistically significant correlations.

### 2.4. Calculation of Correlation Coefficients

We correlate the NAM index with $O/N_2$ at each latitude-longitude grid box to generate correlation maps within the GOLD FOV (approximately 60°S to 60°N in latitude and 110°W to 15°E in longitude) using GOLD $O/N_2$, as

**Table 2**
*Same as Table 1, Except the Number of Days for the Years in Which the WACCM-X Data set Does Not Overlap With GOLD*

| | WACCM-X (2010–2018, 2022) | | | | | | | | | | |
|---|---|---|---|---|---|---|---|---|---|---|---|
| | (2009)–2010 | 2010–2011 | (2011)–2012 | 2012–2013 | (2013)–2014 | 2014–2015 | 2015–2016 | 2016–2017 | 2017–2018 | 2022–(2023) | Total (WACCM-X, 2010–2018) |
| Dates | Jan 1–Mar 23 | Nov 21–Apr 9 | Jan 7–Feb 23 | Nov 26–Feb 1 | Jan 30–Apr 4 | Nov 22–Apr 5 | Dec 6–Mar 24 | Oct 25–Apr 9 | Dec 6–Mar 4 | Nov 27–Dec 31 | n/a |
| Winter days | 80 | 138 | 20 | 66 | 66 | 97 | 110 | 165 | 87 | 26 | 829 |
| Quiet days (Kp < 2.0) | 43 | 64 | 4 | 42 | 30 | 12 | 21 | 45 | 36 | 1 | 297 |
| Anomalous NAM days | 30 | 23 | 3 | 24 | 0 | 8 | 21 | 4 | 17 | 0 | 130 |
| NAM >2.5 days | 0 | 23 | 0 | 0 | 0 | 6 | 5 | 0 | 10 | 0 | 44 |
| NAM < −2.0 days | 30 | 0 | 3 | 24 | 0 | 2 | 16 | 4 | 7 | 0 | 86 |
| Quiet and anomalous NAM | 14 | 10 | 0 | 12 | 0 | 1 | 2 | 0 | 6 | 0 | 45 |

*Note*. WACCM-X data from 27 November 2022 to 31 December 2023 is also shown for completeness.

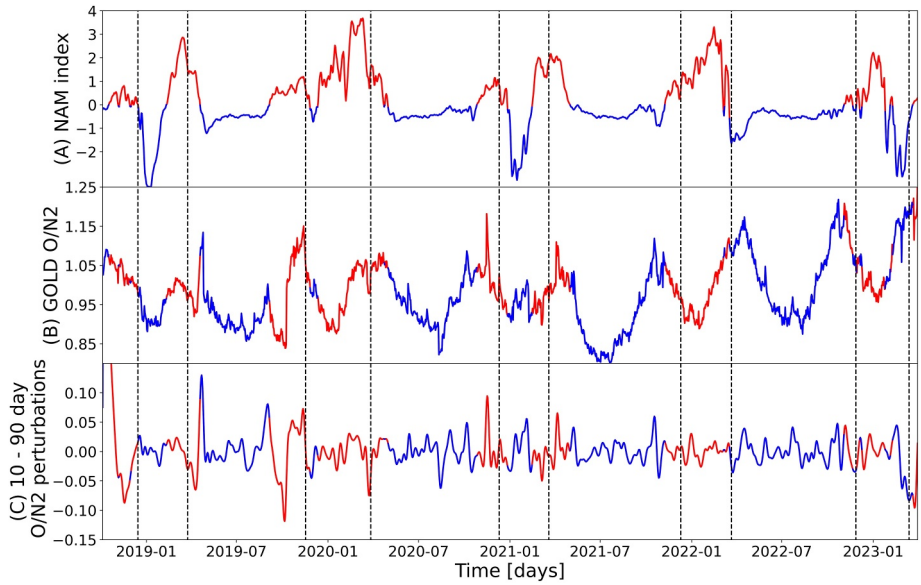


**Figure 1.** (a) 10 hPa northern annular mode (NAM) index. (b) Unfiltered global observations of the limb and disk (GOLD) O/$N_2$, averaged from ± 20° lat. (c) 10- to 90-day perturbations in GOLD O/$N_2$. (a, b), and (c) are all colored by positive (red) and negative (blue) NAM values. The dashed lines in all panels indicate the first and last day of winter, which is defined when the 10 days rolling window standard deviation of the polar vortex exceeds 0.35.

well as global maps using WACCM-X O/$N_2$. For calculations of the correlation coefficient, we omit geomagnetically active days (Kp > 2.0) because O/$N_2$ variability is strongly dependent on geomagnetic activity, and the NAM signal is washed out by the influence of forcing from above during geomagnetically active periods (Martinez & Lu, 2023). The numbers of active PV and quiet geomagnetic activity days, and therefore the number of days used to calculate correlations, are summarized in Tables 1 and 2 (last row). The statistical significance of correlation coefficients is determined using a Student's *t*-test and the associated p-value. We consider correlations where the p-value is less than 0.05, which means that the significance level of the correlation is greater than 95%, to be significant.

## 3. Observations and Results

### 3.1. Sub-Seasonal Variability in O/$N_2$ and NAM

The first row of Figure 1 shows the NAM index at 10 hPa. Winter times, defined using a 10-day rolling window standard deviation, are demarcated with dashed lines. Winters in which there is no SSW, such as 2020 and 2022, show almost entirely positive NAM, indicating a less disturbed and strong PV. SSWs occurred in 2019, 2021, and 2023, and can be seen in the large blue decreases in Figure 1a. The NAM index is not variable during non-winter months when the PV is not active, so these times are not considered in our analysis.

The global distribution of O/$N_2$ has a well-known and well-studied seasonal dependence related to the seasonal dependence of the mean circulation. The seasonal dependence of the PV and mean circulation therefore leads to strong but non-causal correlations between the raw O/$N_2$ ratio and the NAM index. To remove the seasonal variations, we calculate perturbations in the GOLD O/$N_2$ ratio by first subtracting the average value over the five years of available data and then applying a 10- to 90-day fourth-order Butterworth bandpass filter. Figure 1b shows the O/$N_2$ ratio averaged between ±20° latitude, and Figure 1c shows the 10–90 days O/$N_2$ filtered perturbations, which is used for correlation with the NAM index. The wavelet decomposition of the NAM index is shown in Figure 2. In addition to the expected, strong seasonal (>90 days) signals during the winter time, there is significant variability on subseasonal (<90 days) time scales, but relatively weak variability on short (<10 days) timescales, which motivates our selection of 10 days as the cutoff period for our filtering of O/$N_2$ perturbations.



21699402, 2024, 6, Downloaded from https://agupubs.onlinelibrary.wiley.com/doi/10.1029/2024JA032724, Wiley Online Library on [29/07/2024]. See the Terms and Conditions (https://onlinelibrary.wiley.com/terms-and-conditions) on Wiley Online Library for rules of use; OA articles are governed by the applicable Creative Commons License

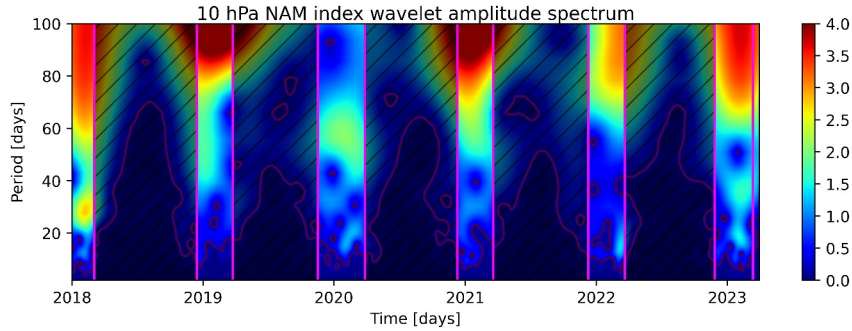


**Figure 2.** Wavelet amplitude spectrum of the 10 hPa northern annular mode index. Solid pink vertical lines are the start and end for each winter. The black curve shows significant amplitudes at the 95% confidence level. Solid pink lines separate different winters, with black hatches partially obscuring non-winter times.

### 3.2. Distribution of $O/N_2$ During Strong and Weak Vortex Times

Figure 3a1 shows the composite of GOLD $O/N_2$ for all geomagnetically quiet (Kp < 2.0) NH winter days with NAM < −2.1 (24 days), indicating a strong/stable PV. Data are binned into 10° × 10° grid boxes with composites being calculated as arithmetic means. Figure 3b1 is the same as Figure 3a1, except for NAM >2.5 (22 days), indicative of a weak PV. Figure 3c1 shows the percentage difference between Figures 3a1 and 3b1, which is the difference between $O/N_2$ during a weak and strong PV. The second row is the same except differences and means are calculated for 10–90 days perturbations, and the difference shown in Figure 3c1 is an absolute difference, rather than a percentage difference.

From column C of Figure 3, it is clear that the global distribution of $O/N_2$ varies with the strength of the PV. In both the unfiltered case (row 1) and on sub-seasonal (row 2) time scales, during a weak vortex, $O/N_2$ is relatively depleted at low and mid-southern latitudes, which is demonstrated by the negative difference (red) in $O/N_2$ over South America (Figures 3c1 and 3c2). At middle and low latitudes, the depletion in $O/N_2$ is qualitatively consistent with the results of Oberheide et al. (2020), which showed depletion of $O/N_2$ at similar latitudes in response to an SSW (when the PV is extremely weak). The positive difference (blue) at mid-to high-northern latitudes is indicative of a relative enhancement in $O/N_2$ at high northern latitudes during a weak PV. Overall

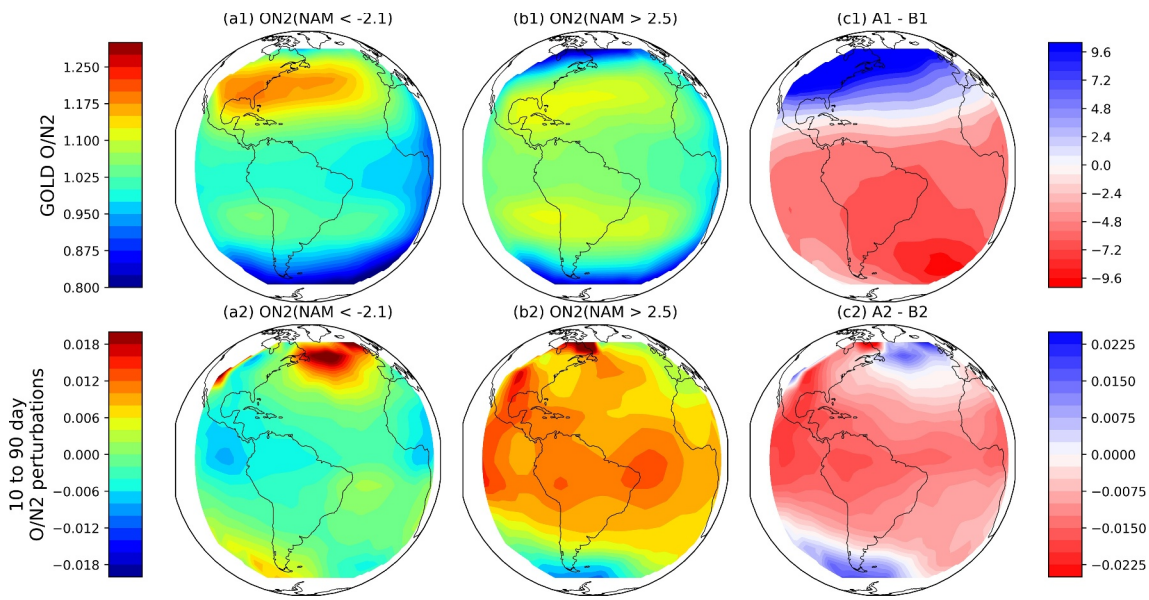


**Figure 3.** (a1) Composite of unfiltered Global Observations of the Limb and Disk $O/N_2$ for geomagnetically quiet days (Kp < 2.0) days in which northern annular mode (NAM) < −2.1. (b1) Is the same as (a1) except for NAM > −2.5. (c1) The percentage difference between (a1) and (b1). Row 2 is the same as row 1, except $O/N_2$ are 10–90 days perturbations, and (c2) shows the absolute difference, rather than the percentage difference.



21699402, 2024, 6, Downloaded from https://agupubs.onlinelibrary.wiley.com/doi/10.1029/2024JA032724, Wiley Online Library on [29/07/2024]. See the Terms and Conditions (https://onlinelibrary.wiley.com/terms-and-conditions) on Wiley Online Library for rules of use; OA articles are governed by the applicable Creative Commons License

21699402, 2024, 6, Downloaded from https://agupubs.onlinelibrary.wiley.com/doi/10.1029/2024JA032724, Wiley Online Library on [29/07/2024]. See the Terms and Conditions (https://onlinelibrary.wiley.com/terms-and-conditions) on Wiley Online Library for rules of use; OA articles are governed by the applicable Creative Commons License

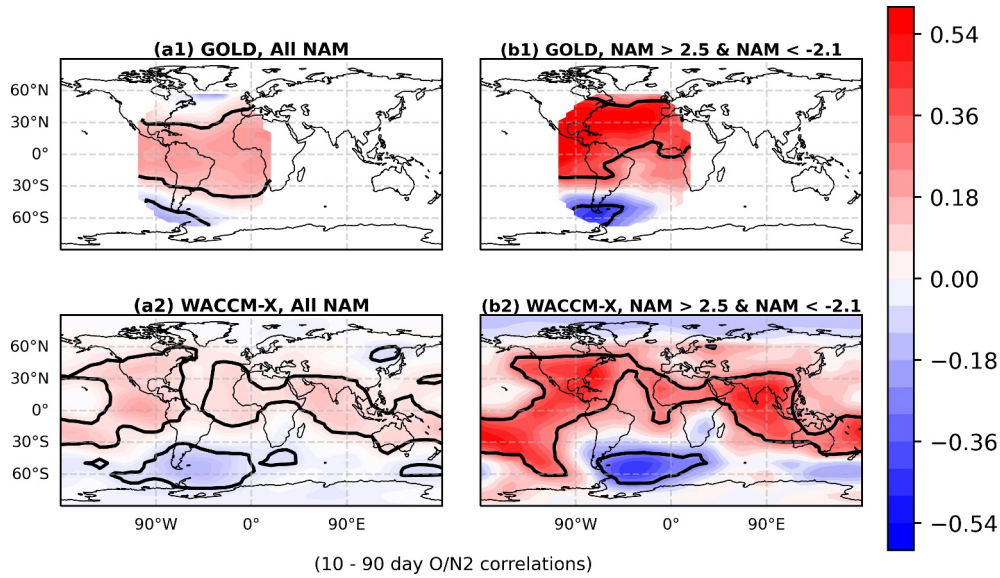


**Figure 4.** (a1) Correlation map for 10–90 days global observations of the limb and disk (GOLD) $O/N_2$ perturbations and the 10 hPa northern annular mode (NAM) index in the GOLD field of view for geomagnetically quiet days during northern hemisphere winter from in 2018–2023 with a 6-day time lag (NAM index leads). Regions where the significance level exceeds 95% are highlighted by the black contour. (a2) Is the same as (a1), except $O/N_2$ perturbations are obtained from Whole Atmosphere Community Climate Model with thermosphere-ionosphere eXtension and winters of 2010–2022 are used. Column b is the same as column a, except days where −2.1 < NAM <2.5 days are omitted.

(without filtering), the weak-versus-strong PV causes an average of ∼10% change for $O/N_2$ (Figure 3c1). The high-latitude enhancement in $O/N_2$ and the low-latitude depletion in $O/N_2$ suggests a change in mean circulation associated with the weak PV, with upwelling and poleward transport at low latitudes and corresponding downwelling at high latitudes. For the latitude range shown in Figure 3, it seems like the seasonal-scale circulation is dominated by a one-cell structure while the sub-seasonal circulation is dominated by a two-cell pattern. The mechanisms responsible for the differences shown in Figure 3c2 are discussed in further detail in Section 4. Note that $O/N_2$ maps generated using WACCM-X, which are not shown, display similar distributions of positive and negative differences.

### 3.3. Correlations Between $O/N_2$ and NAM Variabilities

We correlate $O/N_2$ with the NAM index to further study the influence of the PV on $O/N_2$. It is important that we use the filtered $O/N_2$ because the high correlations between unfiltered $O/N_2$ ratio and NAM mostly originate from their seasonal variations (Figure 1). Figure 4a1 shows the 6-day time-lagged correlation coefficient of 10–90 days $O/N_2$ perturbations with the 10 hPa NAM index in the GOLD FOV during the geomagnetically quiet (Kp < 2.0) NH winter days. Figure 4b1 is the same except that one additional criterion: NAM ≥ 2.5 or NAM ≤ −2.1 (hereafter referred to as "anomalous vortex") is used. The 6-day time lag was chosen because it maximizes the correlations here, which is consistent with a time lag of approximately 1 week used in Pedatella (2023) for the PV modulation on $O/N_2$ in WACCM-X. The second row is the same as the first one except for using WACCM-X data from winters of 2010–2022, with the same analysis as applied to the GOLD data.

We find positive correlations between GOLD $O/N_2$ and the NAM in terms of the sub-seasonal (10–90 days) variabilities in low- and mid-northern latitudes in the GOLD FOV, and in particular correlations as large as +0.55 (at 30°N) when only anomalous vortex times are considered, and +0.22 (at 10°N) when all NAM are considered. The positive correlation means higher $O/N_2$ during more positive NAM and lower ones during more negative NAM, which is consistent with the positive differences of $O/N_2$ at the same latitudes as PV strengthens (Figure 3c2). Where correlations are significant in both GOLD and WACCM-X, there is qualitative agreement between them. For example, the maximum positive correlations (+0.54) from WACCM-X are observed at approximately the same region as in GOLD. At high latitudes anti-correlations, which are strongest in the

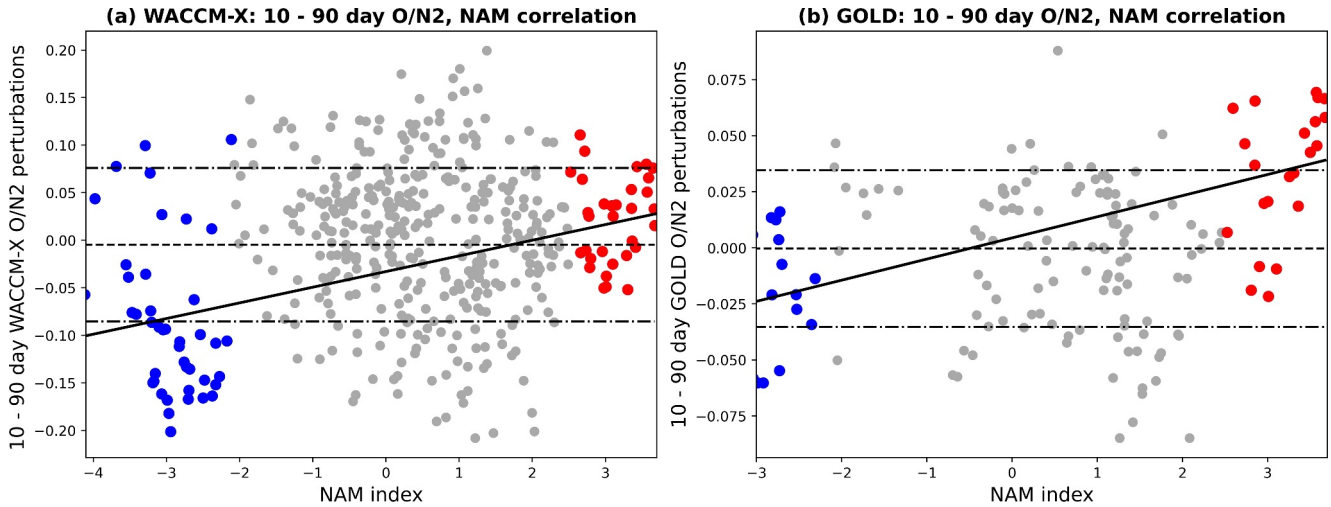


**Figure 5.** (a) 10–90 days whole atmosphere community climate model with thermosphere-ionosphere eXtension $O/N_2$ perturbations at (30°N, 110°W), as a function of the northern annular mode (NAM) index for geomagnetically quiet (Kp < 2.0) winter days. Anomalous vortex days NAM >2.5 and NAM < −2.1 are marked by red and blue points, respectively. The horizontal lines near 0 show the average of all perturbations. The horizontal lines above and below this line show one standard deviation above and below the mean. (b) Is the same as (a) except $O/N_2$ perturbations are obtained from Global Observations of the Limb and Disk at (30°N, 90°W.).

southern hemisphere, are found in both GOLD and WACCM-X. For example, when only anomalous vortex events are considered, an anti-correlation of −0.52 is found at 60°S in WACCM-X, compared to −0.54 in GOLD.

Now, we focus our analysis to a region in which particularly strong correlations are observed. Figure 5a shows the relationship between the 10–90 days WACCM-X $O/N_2$ perturbations at (30°N, 110°W) and the 10 hPa NAM index. Figure 5b is the same as 5A, except the $O/N_2$ is from GOLD at (30°N, 90°W). The correlation coefficient between $O/N_2$ and NAM at this location is +0.55 in GOLD and +0.54 in WACCM-X when only geomagnetically quiet and anomalous vortex days are included (red and blue dots). The $O/N_2$ ratio becomes less correlated with the NAM index when −2.1 < NAM <2.5 days are included (gray dots), as the correlation coefficient drops to +0.22 and + 0.18 in GOLD and WACCM-X, respectively, when all days are considered regardless of vortex strength. The parameters become decorrelated for −2.1< NAM <2.5 because $O/N_2$ is highly sensitive to many other forcings, such as weak geomagnetic activity, which wash out the PV signal when the vortex is inactive (i.e., neither particularly strong nor particularly weak).

In GOLD, 67% of $O/N_2$ perturbations are negative when NAM < −2.1%, and 27% are more than 1 sigma lower than the mean. In other words, GOLD $O/N_2$ perturbations are usually negative when the vortex is very weak. For strong vortex times, when NAM >2.5, 82% of GOLD $O/N_2$ perturbations are positive, 55% of $O/N_2$ perturbations are greater than 1 sigma above the mean, and 0% of the perturbations are less than 1 sigma below the mean. The strong vortex is, therefore, a more reliable predictor of $O/N_2$ enhancement at low to mid-latitudes than the weak vortex is of $O/N_2$ depletion, but $O/N_2$ is still generally depleted during weak vortex times. Similar patterns are apparent in the statistics of the WACCM-X perturbation. The statistics derived from WACCM-X are more robust than those derived from GOLD since the WACCM-X data set is more than twice as large as the GOLD data set, but the agreement between the two sets of results indicates that both are reliable. These statistics are summarized in Table 3.

## 4. Coupling Polar Vortex Signals to Thermospheric $O/N_2$ via Residual Mean Meridional Circulation

As mentioned in Section 1, wave activity (tides, gravity waves, and planetary waves) are known to be impacted by PV activity, and these waves are known to impact circulation and composition in the lower thermosphere. On sub-seasonal time scales, our correlations at mid -to -low northern and southern latitudes are consistent with and therefore provide evidence for the theory (e.g., Yamazaki & Richmond, 2013) that the PV impacts modify the background zonal mean zonal winds, thereby modifying the tides, and the ensuing changes in tidal breaking impacts circulation to induce upwelling at low latitudes (Oberheide et al., 2020) and corresponding downwelling



21699402, 2024, 6, Downloaded from https://agupubs.onlinelibrary.wiley.com/doi/10.1029/2024JA032724, Wiley Online Library on [29/07/2024]. See the Terms and Conditions (https://onlinelibrary.wiley.com/terms-and-conditions) on Wiley Online Library for rules of use; OA articles are governed by the applicable Creative Commons License

21699402, 2024, 6, Downloaded from https://agupubs.onlinelibrary.wiley.com/doi/10.1029/2024JA032724, Wiley Online Library on [29/07/2024]. See the Terms and Conditions (https://onlinelibrary.wiley.com/terms-and-conditions) on Wiley Online Library for rules of use; OA articles are governed by the applicable Creative Commons License

**Table 3**
*Statistical Distribution of 10–90 Days O/$N_2$ Perturbations in GOLD and WACCM-X With Respect to the 10 hPa Northern Annular Mode Index in GOLD and WACCM-X at a Location of (30°N, 110°W)*

| | 10–90 days O/$N_2$ perturbations | | | | | |
|---|---|---|---|---|---|---|
| | NAM <−2.1 | | NAM >−2.1, NAM <+2.5 | | NAM >+2.5 | |
| % Of anomalies… | GOLD | WACCM-X | GOLD | WACCM-X | GOLD | WACCM-X |
| … > mean | 33% | 19% | 53% | 56% | 82% | 63% |
| … < mean | 67% | 81% | 47% | 44% | 18% | 37% |
| … > mean + 1 sigma | 0% | 7% | 8% | 16% | 55% | 34% |
| … < mean −1 sigma | 27% | 62% | 21% | 14% | 0% | 0% |

*Note*. Text is colored blue to emphasize periods in which weak NAM corresponds to an O/$N_2$ depletion (relative to the mean), and colored dark red when a strong NAM corresponds to an O/$N_2$ enhancement.

at high latitudes during a weakened PV. Given the strong latitudinal agreement between GOLD and WACCM-X correlations with the NAM index, as well as the relative lack of longitudinal variations in terms of sign (correlations are generally positive at low latitudes and negative at high latitudes across all longitudes), we now use residual mean meridional circulation (MMC) calculated from WACCM-X to confirm that the correlation map in O/$N_2$ reflects PV induced variations in the residual MMC.

The vector field in Figure 6 shows the difference between the average residual MMC for anomalously weak (NAM < −2.1) and anomalously strong (NAM >2.5) vortex, geomagnetically quiet (Kp < 2.0) times. The x-component of each vector is given by the meridional component of the residual MMC, $\overline{v}^*$, and the y-component is given by the vertical component of the residual MMC, $\overline{w}^*$. $\overline{v}^*$ and $\overline{w}^*$ are given by (Andrews et al., 1987),

$$\overline{v}^* = \overline{v} - \frac{1}{\rho}\frac{\partial}{\partial z}\left(\rho \frac{\overline{v'\theta'}}{\overline{\theta}_z}\right)$$

$$\overline{w}^* = \overline{w} + \frac{1}{a\cos\phi}\frac{\partial}{\partial \phi}\left(\cos\frac{\overline{v'\theta'}}{\overline{\theta}_z}\right)$$

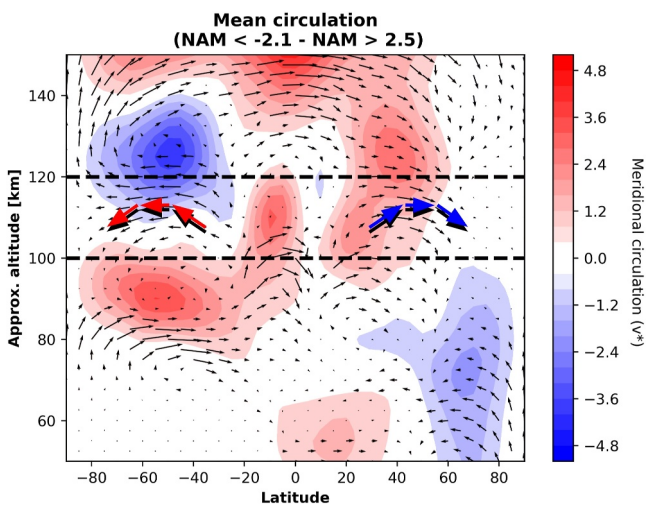


**Figure 6.** Differential residual mean meridional circulation (MMC), that is, residual MMC during weak vortex times (Northern Annular Mode < −2.1) minus that during strong vortex times (NAM> 2.5). The contours show only the meridional component of the residual MMC. Composites also include 6 days after an anomalous vortex event, but omit geomagnetically active days (Kp > 2.0.). The dashed black lines indicate the approximate altitude at which circulation changes map to O/$N_2$ variations. The thick blue and red arrows are drawn to highlight a weak vortex induced, neutral air "fountain."

where φ is the latitude, $a$ is the radius of the Earth, ρ is atmospheric density, barred values indicate zonal means, and values with tick marks are perturbations from the zonal mean. The color contours in Figure 6 show the difference between the meridional components of the residual MMC, $\overline{v}^*$ (negative/blue is southward motion, positive/red is northward motion). In order to account for the 6-day time lag that was determined to maximize the response between the NAM index and O/$N_2$ perturbations, we include the 6 days following each anomalously weak/strong vortex time in each composite. All geomagnetically active days (Kp > 2.0) are still omitted. After applying these criteria, the strong vortex composite includes 83 days, and the weak vortex composite includes 113 days.

Figure 6 is generated by subtracting the strong vortex composite from the weak vortex composite, so the vectors/colors shown in Figure 6 can be thought of as illustrating the response of the mean circulation to a dramatically weakened vortex. In the lower thermosphere, (approximately 100–120 km, demarcated with dashed black lines), we observe enhanced upwelling at low latitudes, with corresponding poleward transport at mid-latitudes and downwelling at high latitudes (somewhat analogous to the

21699402, 2024, 6, Downloaded from https://agupubs.onlinelibrary.wiley.com/doi/10.1029/2024JA032724, Wiley Online Library on [29/07/2024]. See the Terms and Conditions (https://onlinelibrary.wiley.com/terms-and-conditions) on Wiley Online Library for rules of use; OA articles are governed by the applicable Creative Commons License

ionospheric "fountain effect") This pattern is highlighted with two sets of arrows (thick red and blue with black shadows) drawn over the vector field. This upwelling is the result of a large cell of enhanced counterclockwise circulation in the southern hemisphere approximately centered at 50°S and 110 km (see the large regions of southward $\overline{v}^*$ above and northward $\overline{v}^*$ below this location), as well as a less dramatic cell of enhanced clockwise circulation in the northern hemisphere, centered around 40°N.

By comparison with Figure 4, we can see strong qualitative agreement with the structure of the $O/N_2$-NAM correlation map. The region of $O/N_2$-NAM anti-correlations, which we attribute to vortex induced downwelling, is centered over 50°S, which is consistent with the downwelling shown in Figure 6. There are positive correlations at low latitudes, which are consistent with upwelling at low latitudes shown in Figure 6. Additionally, there are statistically non-significant anti-correlations at high northern latitudes, which is consistent with the relatively weaker vortex induced downwelling occurring at high northern latitudes.

## 5. Discussion

The NAM index is positively correlated with $O/N_2$ within much of the GOLD FOV, and, based on WACCM-X simulations, negatively correlated at high latitudes. These results support the hypothesis that the PV is related to IT variability via wave activity in the lower atmosphere. The following example can explain the correlations: A weak PV is indicated by a negative NAM index. As the PV is weakened, zonal mean zonal winds flow increasingly in the westward direction. This leads to enhancements in the strength of the westward propagating waves, including, for example, tidal components such as SW2 and westward migrating planetary waves, at low- and mid-latitudes. The dissipation of these enhanced tides at midlatitudes induces poleward circulation, which enhances upwelling (of O-poor/$N_2$-rich air from the lower atmosphere) at mid to low latitudes (hence a decrease in $O/N_2$, hence the positive correlations between $O/N_2$ and NAM in Figures 4 and 5, and enhances downwelling at high northern and mid-to-high southern latitudes (hence an increase in $O/N_2$.)

The patterns shown in residual MMC here are consistent with the results of Zhang et al. (2024), who used the velocity stream function of the residual MMC to demonstrate SSW induced reversals of MMC in the lower thermosphere during two SSW events (December 2018 and January 2021). They attributed the circulation reversals to perturbations of westward-propagating planetary waves, and found that forcing from tides and gravity waves play a comparatively smaller role. The strong agreement between statistical results presented here and the case study of Zhang et al. (2024) suggests that westward-propagating planetary waves are also the dominant drivers of the circulation changes shown in Figure 6.

Additionally, gravity wave forcing near the mesosphere is responsible for the summer-to-winter residual circulation in the mesosphere and a corresponding winter-to-summer residual circulation in the lower thermosphere (Garcia & Solomon, 1985; Holton, 1983; Lindzen, 1981; Qian & Yue, 2017). At the same time, gravity wave activity is strongly dependent on the PV, and it acts to modulate the effectiveness of gravity wave propagation into the mesosphere thermosphere as well as generate secondary gravity waves (Harvey et al., 2022) Modulations in the strength of the PV should therefore also be expected to induce perturbations in residual thermospheric circulation via gravity waves, which would also be reflected in the global distribution of $O/N_2$. Recently, Liu et al. (2024) used a high resolution version of WACCM-X to demonstrate that forcing from relatively small scale gravity waves, which are not presented in the standard version of SD-WACCM-X used here, impact circulation in the lower thermosphere and the ratio of $O/N_2$. A study of the relative contributions of gravity wave, tidal, and planetary wave activity to residual circulation (and $O/N_2$) variance during anomalous PV times would, therefore, require a version of WACCM-X capable of resolving gravity waves, and is therefore left as a goal for future research.

## 6. Conclusions

In summary, we study the sub-seasonal (10–90 days) variability of $O/N_2$ using GOLD (limited FOV) and we use WACCM-X to extend the study for other regions, especially high latitudes. We investigate the impacts of the PV on these variabilities during geomagnetically quiet, anomalous vortex times. We demonstrate that the PV drives changes in the composition ($O/N_2$) of the lower thermosphere. On 10–90 days time scales, the NAM index is positively correlated (+0.55) with GOLD observations of the $O/N_2$ ratio at low and middle latitudes, and negatively correlated (−0.54) at high southern latitudes. These correlations reflect a PV induced neutral air

21699402, 2024, 6, Downloaded from https://agupubs.onlinelibrary.wiley.com/doi/10.1029/2024JA032724, Wiley Online Library on [29/07/2024]. See the Terms and Conditions (https://onlinelibrary.wiley.com/terms-and-conditions) on Wiley Online Library for rules of use; OA articles are governed by the applicable Creative Commons License

"fountain," in which upwelling is enhanced at low latitudes with corresponding down welling and poleward transport at high latitudes.

The primary mechanisms responsible for the coupling of the stratospheric PV to thermospheric composition is likely the modulation of tides, gravity waves, and planetary waves via vortex induced changes in the background zonal mean zonal wind. Momentum deposition resulting from the dissipation of these modified waves causes changes in residual MMC, with a particularly notable feature being enhanced upwelling at low latitudes and corresponding downwelling at high latitudes (in both hemispheres.) These perturbations in circulation are then ultimately mapped to higher altitudes via molecular diffusion and ultimately into the global distribution of $O/N_2$.

## Data Availability Statement

Publicly available data sets were analyzed in this study. GOLD $O/N_2$ data can be found here: https://gold.cs.ucf.edu/data/search/ and here: https://cdaweb.gsfc.nasa.gov/pub/data/gold/ (long term archive). WACCM-X is part of the Community Earth System Model (CESM) and the source code is available at https://github.com/ESCOMP/CESM. The $O/N_2$ ratio and residual MMC from SD-WACCMX is available at https://clemson.box.com/s/4pte9n76yxcqhl5g4b3r3zwzvvhvey45. MERRA-2 data is available at https://goldsmr5.gesdisc.eosdis.nasa.gov/data/MERRA2/M2I6NVANA.5.12.4/.

**Acknowledgments**
B.C.M. and X.L.'s work is supported by NASA 80NSSC22K0018, NNX17AG10G, 80NSSC22K1010, 80NSSCK19K0810, and NSF AGS-2149695 (ANSWERS) and CAREER-1753214, and AGS-2012994. This material is based upon work supported by the NSF National Center for Atmospheric Research, which is a major facility sponsored by the U.S. National Science Foundation under Cooperative Agreement 1852977. N.P. and J.O. acknowledge support from NASA Grant 80NSSC20K1353. N.P. also acknowledges support from NASA Grant 80NSSC23K0418.

## References

Andrews, D. G., Holton, J. R., & Leovy, C. B. (1987). *Middle atmosphere dynamics*. Academic Press.

Baldwin, M. P. (2001). Annular modes in global daily surface pressure. *Geophysical Research Letters*, *28*(21), 4115–4118. https://doi.org/10.1029/2001gl013564

Baldwin, M. P., Ayarzagüena, B., Birner, T., Butchart, N., Butler, A. H., Charlton-Perez, A. J., et al. (2021). Sudden stratospheric warmings. *Reviews of Geophysics*, *59*(1), e2020RG000708. https://doi.org/10.1029/2020RG000708

Correira, J., Evans, J. S., Lumpe, J. D., Krywonos, A., Daniell, R., Veibell, V., et al. (2021). Thermospheric composition and solar EUV flux from the global-scale observations of the limb and disk (GOLD) mission. *Journal of Geophysical Research: Space Physics*, *126*(12), e2021JA029517. https://doi.org/10.1029/2021JA029517

Eastes, R. W., McClintock, W. E., Burns, A. G., Anderson, D. N., Codrescu, M., Correira, J. T., et al. (2017). The global-scale observations of the limb and disk (GOLD) mission. *Space Science Reviews*, *212*(1–2), 383–408. https://doi.org/10.1007/s11214-017-0392-2

England, S. L., Greer, K. R., Zhang, S.-R., Evans, S., Solomon, S. C., Eastes, R. W., et al. (2021). First comparison of traveling atmospheric disturbances observed in the middle thermosphere by global-scale observations of the limb and disk to traveling ionospheric disturbances seen in ground-based total electron content observations. *Journal of Geophysical Research: Space Physics*, *126*(6), e2021JA029248. https://doi.org/10.1029/2021JA029248

England, S. L., Immel, T. J., Huba, J. D., Hagan, M. E., Maute, A., & DeMajistre, R. (2010). Modeling of multiple effects of atmospheric tides on the ionosphere: An examination of possible coupling mechanisms responsible for the longitudinal structure of the equatorial ionosphere. *Journal of Geophysical Research*, *115*(A5), 05308. https://doi.org/10.1029/2009JA014894

England, S. L., Meier, R. R., Frey, H. U., Mende, S. B., Stephan, A. W., Krier, C. S., et al. (2021). First results from the retrieved column $O/N_2$ ratio from the ionospheric connection explorer (ICON): Evidence of the impacts of nonmigrating tides. *Journal of Geophysical Research: Space Physics*, *126*(9), e2021JA029575. https://doi.org/10.1029/2021JA029575

Garcia, R. R., & Solomon, S. (1985). The effect of breaking gravity waves on the dynamics and chemical composition of the mesosphere and lower thermosphere. *Journal of Geophysical Research*, *90*(D2), 3850–3868. https://doi.org/10.1029/JD090iD02p03850

Gelaro, R., McCarty, W., Suárez, M. J., Todling, R., Molod, A., Takacs, L., et al. (2017). The Modern-Era Retrospective analysis for research and applications, version 2 (MERRA-2). *Journal of Climate*, *30*(14), 5419–5454. https://doi.org/10.1175/JCLI-D-16-0758.1

Gerber, E. P., & Martineau, P. (2018). Quantifying the variability of the annular modes: Reanalysis uncertainty vs. sampling uncertainty. *Atmospheric Chemistry and Physics*, *18*(23), 17099–17117. https://doi.org/10.5194/acp-18-17099-2018

Goncharenko, L. P., Harvey, V. L., Greer, K. R., Zhang, S.-R., Coster, A. J., & Paxton, L. J. (2021). Impact of September 2019 Antarctic sudden stratospheric warming on mid-latitude ionosphere and thermosphere over North America and Europe. *Geophysical Research Letters*, *48*(15), e2021GL094517. https://doi.org/10.1029/2021GL094517

Greer, K. R., Goncharenko, L. P., Harvey, V. L., & Pedatella, N. (2023). Polar vortex strength impacts on the longitudinal structure of thermospheric composition and ionospheric electron density. *Journal of Geophysical Research: Space Physics*, *128*(9), e2023JA031797. https://doi.org/10.1029/2023JA031797

Harvey, V. L., Randall, C. E., Bailey, S. M., Becker, E., Chau, J. L., Cullens, C. Y., et al. (2022). Improving ionospheric predictability requires accurate simulation of the mesospheric polar vortex. *Frontiers in astronomy and space sciences*, *9*, 1041426. https://doi.org/10.3389/fspas.2022.1041426

Holton, J. R. (1983). The influence of gravity wave breaking on the general circulation of the middle atmosphere. *Journal of the Atmospheric Sciences*, *40*(10), 2497–2507. https://doi.org/10.1175/1520-0469(1983)040<2497:tiogwb>2.0.co;2

Labitzke, K., & Naujokat, B. (2000). *The lower arctic stratosphere in winter since 1952*. (Vol. 15, pp. 11–14). SPARC Newsl. Retrieved from https://www.atmosp.physics.utoronto.ca/SPARC/News15/15_Labitzke.html

Lindzen, R. S. (1981). Turbulence and stress owing to gravity wave and tidal breakdown. *Journal of Geophysical Research*, *86*(C10), 9707–9714. https://doi.org/10.1029/JC086iC10p09707

Liu, G., Rowland, D. E., Gan, Q., Liu, H.-L., Klenzing, J. H., England, S. L., & Eastes, R. W. (2023). Thermospheric temperature and $\Sigma O/N_2$ variations as observed by GOLD and compared to MSIS and WACCM-X simulations during 2019-2020 at deep solar minimum. *Journal of Geophysical Research: Space Physics*, *128*(6), e2023JA031560. https://doi.org/10.1029/2023JA031560

Liu, H.-L., Bardeen, C. G., Foster, B. T., Lauritzen, P., Liu, J., Lu, G., et al. (2018). Development and validation of the whole atmosphere community climate model with thermosphere and ionosphere extension (WACCM-X 2.0). *Journal of Advances in Modeling Earth Systems*, *10*(2), 381–402. https://doi.org/10.1002/2017MS001232

Liu, H.-L., Lauritzen, P. H., & Vitt, F. (2024). Impacts of gravity waves on the thermospheric circulation and composition. *Geophysical Research Letters*, *51*(3), e2023GL107453. https://doi.org/10.1029/2023GL107453

Luan, X., Wang, W., Burns, A., & Dou, X. (2017). Solar cycle variations of thermospheric $O/N_2$ longitudinal pattern from TIMED/GUVI. *Journal of Geophysical Research: Space Physics*, *122*(2), 2605–2618. https://doi.org/10.1002/2016JA023696

Martinez, B. C., & Lu, X. (2023). Quantifying day-to-day variability of $O/N_2$ and its correlation with geomagnetic activity using GOLD. *Frontiers in Astronomy and Space Sciences*, *10*, 1129279. https://doi.org/10.3389/fspas.2023.1129279

Matsuno, T. (1971). A dynamical model of the stratospheric sudden warming. *Journal of the Atmospheric Sciences*, *28*(8), 1479–1494. https://doi.org/10.1175/1520-0469(1971)028<1479:ADMOTS>2.0.CO;2

Oberheide, J., Pedatella, N. M., Gan, Q., Kumari, K., Burns, A. G., & Eastes, R. W. (2020). Thermospheric composition O/N response to an altered meridional mean circulation during sudden stratospheric warmings observed by GOLD. *Geophysical Research Letters*, *47*(1), e2019GL086313. https://doi.org/10.1029/2019gl086313

Pedatella, N. M. (2023). Influence of stratosphere polar vortex variability on the mesosphere, thermosphere, and ionosphere. *Authorea Preprints*, *128*(7). https://doi.org/10.1029/2023ja031495

Pedatella, N. M., & Harvey, V. L. (2022). Impact of strong and weak stratospheric polar vortices on the mesosphere and lower thermosphere. *Geophysical Research Letters*, *49*(10), e2022GL098877. https://doi.org/10.1029/2022gl098877

Pedatella, N. M., Richmond, A. D., Maute, A., & Liu, H. L. (2016). Impact of semidiurnal tidal variability during SSWs on the mean state of the ionosphere and thermosphere. *Journal of Geophysical Research: Space Physics*, *121*(8), 8077–8088. https://doi.org/10.1002/2016JA022910

Qian, L., & Yue, J. (2017). Impact of the lower thermospheric winter-to-summer residual circulation on thermospheric composition. *Geophysical Research Letters*, *44*(9), 3971–3979. https://doi.org/10.1002/2017GL073361

Strickland, D. J., Evans, J. S., & Paxton, L. J. (1995). Satellite remote sensing of thermospheric $O/N_2$ and solar EUV: 1. Theory. *Journal of Geophysical Research*, *100*(A7), 12217–12226. https://doi.org/10.1029/95ja00574

Thompson, D. W. J., & Wallace, J. M. (2000). Annular modes in the extratropical circulation. Part I: Month-to-month variability. *Journal of Climate*, *13*(5), 1000–1016. https://doi.org/10.1175/1520-0442(2000)013<1000:AMITEC>2.0.CO;2

Yamazaki, Y., & Richmond, A. D. (2013). A theory of ionospheric response to upward-propagating tides: Electrodynamic effects and tidal mixing effects. *Journal of Geophysical Research: Space Physics*, *118*(9), 5891–5905. https://doi.org/10.1002/jgra.50487

Yu, T., Ren, Z., Le, H., Wan, W., Wang, W., Cai, X., & Li, X. (2020). Seasonal variation of $O/N_2$ on different pressure levels from GUVI limb measurements. *Journal of Geophysical Research: Space Physics*, *125*(8), e2020JA027844. https://doi.org/10.1029/2020JA027844

Zhang, J., Oberheide, J., Pedatella, N. M., & Liu, G. (2024). Impact of Arctic and Antarctic sudden stratospheric warmings on thermospheric composition. *ESS Open Archive*.

Zhang, Y., England, S., & Paxton, L. J. (2010). Thermospheric composition variations due to nonmigrating tides and their effect on ionosphere. *Geophysical Research Letters*, *37*(17), L17103. https://doi.org/10.1029/2010GL044313



21699402, 2024, 6, Downloaded from https://agupubs.onlinelibrary.wiley.com/doi/10.1029/2024JA032724, Wiley Online Library on [29/07/2024]. See the Terms and Conditions (https://onlinelibrary.wiley.com/terms-and-conditions) on Wiley Online Library for rules of use; OA articles are governed by the applicable Creative Commons License